Progress in Natural Science: Materials International 2012;22(1):40–47

Chinese Materials Research Society

Progress in Natural Science: Materials International

www.elsevier.com/locate/pnsmi
www.sciencedirect.com

ORIGINAL RESEARCH

Evaluation of plasma sprayed YSZ thermal barrier coatings with the CMAS deposits infiltration using impedance spectroscopy

Jing Wu, Hongbo Guo*, Musharaf Abbas, Shengkai Gong

Key Laboratory of Aerospace Materials & Performance (Ministry of Education), School of Materials Science and Engineering, Beihang Univerisity, No. 37 Xueyuan Road, Beijing 100191, China

Received 10 November 2011; accepted 17 December 2011
Available online 9 February 2012

KEYWORDS

Calcium–magnesium–alumino-silicate;
Thermal barrier coatings;
Plasma spray;
Impedance spectroscopy

Abstract The yttria-stabilized zirconia (YSZ) thermal barrier coatings (TBCs) prepared by atmospheric plasma spraying with different heat treatment period at the temperature of 1250 °C were studied in the present investigation. Electrochemical impedance spectroscopy (EIS) was employed to non-destructively examine the impedance and capacitance behavior of free standing YSZ coatings deposited by plasma spray with CMAS (calcium–magnesium–alumino-silicate) infiltration. Equivalent circuit was established on the basis of the biomodal structure in coatings. The sintering behavior of the coatings can be reflected by the changes of resistance and capacitance of the coating. By EIS, the microstructure evolution of the coating with CMAS deposits was discussed in detail.

1. Introduction

Thermal barrier coatings (TBCs) are widely used to improve the durability of hot section components in gas turbine engines [1–4]. A typical TBC system consists of a ceramic topcoat for thermal insulation, a thermally grown oxide (TGO) scale, predominantly Al_2O_3, a metallic bond coat providing oxidation and hot corrosion resistance and a superalloy substrate, which is the load-bearing component. Since zirconia has low thermal conductivity and high thermal expansion coefficient, the zirconia partially stabilized with yttria (YSZ) is usually used as ceramic topcoat of TBCs [5].

TBCs used in turbine blades of aircraft engines are subjected to the aggressive combustion environment combined with air-ingested foreign particles. These particles deposit on the hot

*Corresponding author. Tel.: +86 10 8231 7118; fax: +86 10 8233 7117.
E-mail address: clover-tree@163.com (H. Guo).

Peer review under responsibility of Chinese Materials Research Society.
doi:10.1016/j.pnsc.2011.12.007

Production and hosting by Elsevier

TBC surfaces as molten calcium–magnesium–alumino-silicate (CMAS) and infiltrate into the porous TBCs surface of the blades. When the temperature drops, these environmental deposits crystallize and cause the thermal expansion mismatch between CMAS and the coating, thereby leading to the TBCs degradation. This new kind of failure mode of TBCs has attracted a lot of attention in recent years [6–9].

The composition of CMAS in TBC coatings varies in the different place of the world depending on the environment in which TBCs are subjected. CMAS damage to TBCs has been investigated in detail by Mercer et al. [10], Krämer et al. [11], Li et al. [12], Chen [13] and Drexler et al. [14]. Some efforts have been made to improve the resistance of TBCs to high-temperature attack by glassy deposits [15,16].

The non-destructive evaluation techniques are being used for left-life assessment, quality control and life prediction of TBCs [17]. One of these techniques is impedance spectroscopy, which has been widely used for evaluation of TBCs in recent years [18–22]. The main concern of previous studies was to focus on the changes in electrical behavior of TBCs, which are caused by the TGO growth. However, the sintering behavior of ceramic top coating is one important issue for TBCs failure. There is very limited and even virtually no literature available on the evaluation of sintering behavior of TBCs and analysis of CMAS deposits using EIS technique.

In this study, the electrical behavior of free standing YSZ ceramic coating with different heat treatment times is investigated. Since the YSZ coating sinters quickly in early 10 h exposure to high temperature [23], different electrical behaviors for 0 h, 5 h and 10 h after sintering are studied. Based on these results, a new equivalent circuit was established to fit the EIS results. It is probably the first attempt to investigate the APS coating with CMAS infiltration using non-destructive impedance spectroscopy.

2. Experiment procedures

2.1. The preparation of free standing samples

The coating samples were prepared by Metco 7 M atmospheric plasma spray facility with 9 MB spray pistol and Metco 4MP-dual type feedstock system on stainless steel. Free-standing YSZ coating specimens were produced by removing the coatings from the substrates using hydrochloric acid [24].

2.2. Heat treatment

Heat treatment of free-standing coating specimens with CMAS deposits was performed in a muffle furnace. The specimens were heated in the furnace to 1250 °C and held at 1250 °C for different times with and without CMAS deposits. The heating and cooling rate was 6 °C/min. The temperature for heat-treatment was selected based on the melting temperature of CMAS deposits reported by Krämer et al. [11].

2.3. Impedance measurement

Both sides of the YSZ coatings were coated with a platinum paint on an area of 5×5 mm^2, which served as the electrode. The paint was cured at 800 °C for 15 min. Impedance measurements were conducted at 400 °C using a Solartron SI 1255 HF frequency response analyzer coupled with a computer-controlled Solartron 1296 Dielectric Interfaces. Alternating current (AC) amplitude of 10 mV was employed and the AC frequency was in the range of 10^{-1}–10^{7} Hz. Spectra analysis (fitting) was performed using Zview impedance analysis software (Scribner Associates Inc., Southern Pines, NC, USA) to obtain the electrical properties of YSZ coatings. After impedance measurement, microstructure of the specimens was analyzed by a CS3400 scanning electron microscope (SEM) equipped with energy dispersive spectroscopy.

3. Results and discussion

3.1. Microstructure and EIS characterization of as-sprayed YSZ coating monolithic

The microstructure of the air plasma sprayed coating is quite complex. The porosity distribution of coating revealed a typical bimodal distribution of semi-molten particles' zones and the lamellar columnar crystals' molten zones as shown in Fig. 1. For the structured YSZ coating, the semi-molten zones consist of the un-molten particles, which retained their nano-size.

Impedance diagrams were obtained by measuring the magnitude and phase shift of the resultant current. There were two types of impedance diagrams, namely Nyquist plots in Fig. 2 and Bode plots in Fig. 3. In a Nyquist plot, the impedance was represented by a real part Z' and an imaginary part Z'' with the formula: $Z(w)=Z'+Z''$. Therefore, the Nyquist plot was also termed as the complex plane impedance plot. For a simple resistor–capacitor (R–C) circuit, the Nyquist plot was characterized by a semicircle. Usually, the Nyquist plot is used to determine the major parameters, such as resistance and capacitance corresponding to an electrochemical system. In a Nyquist plot that contains only one semicircle, the resistance value, R, is determined directly from the intercept with the real Z axis. If the system is complicated, there may be a few semicircles present. For the

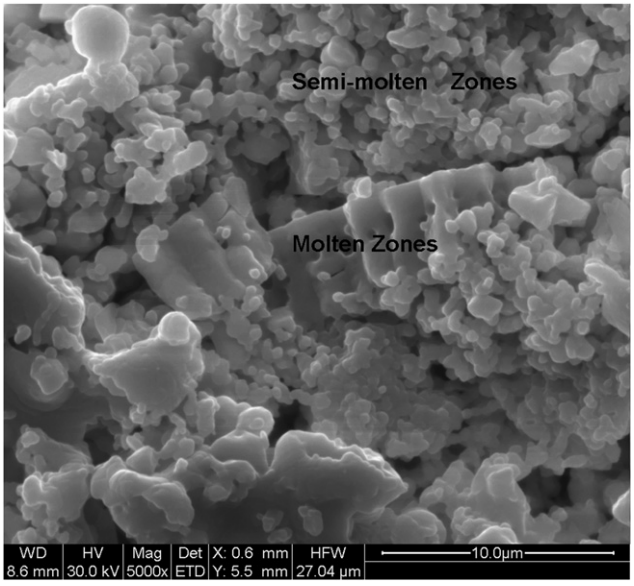

Fig. 1 Fracture morphology of a typical air plasma sprayed TBC.

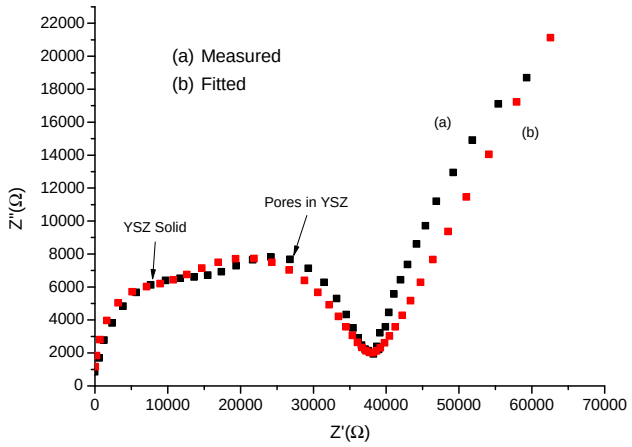

Fig. 2 Measured Nyquist impedance spectra (a) and fitted result (b) of as-sprayed YSZ coating.

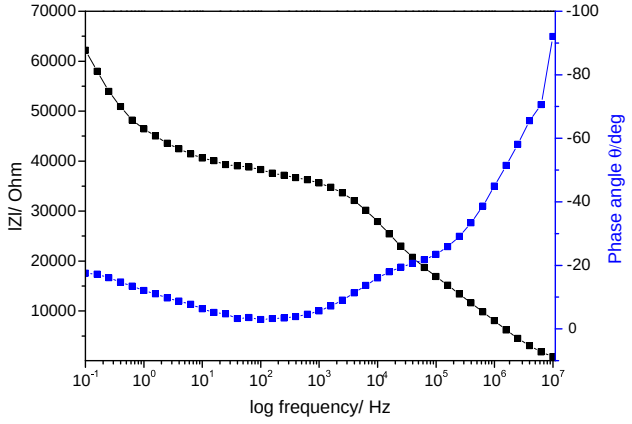

Fig. 3 Impedance Bode plots' spectra of as-sprayed YSZ coatings.

free standing YSZ coating, the Nyquist plot contains two semicircles, which represents two constants. As mentioned previously, the APS YSZ has typical bimodal structure, therefore the two semicircles correspond to the resistance of semi-molten parts and molten parts, as shown in Fig. 2. The phase angles and $|Z|$ as a function of frequency in a Bode plot are shown in Fig. 3. There is one relaxation process (characterized by inflections) for the specimen. From Fig. 3, the three time constants correspond to (1) the molten YSZ (RYSZ · CYSZ) whose frequency range is approximately at 0.3–0.6 MHz, (2) the porous semi-molten part in the YSZ (RP · CP) whose frequency is approximately 1 Hz and (3) the charge transfer resistance that is presented at the frequency of $1–10^{-2}$ MHz [25].

Based on aforementioned study, an AC equivalent circuit for the free standing as-sprayed YSZ coating was developed and is shown in Fig. 4. Since the irregular YSZ surface may give rise to the frequency dispersion and non-uniform distribution in the current density [26], the circuit consists of constant phase elements (CPE) in place of an ideal capacitor. In the present study, the three time constants correspond to the molten YSZ (RYSZ · CYSZ) whose frequency range is approximately at 0.3–0.6 MHz, the porous semi-molten in the

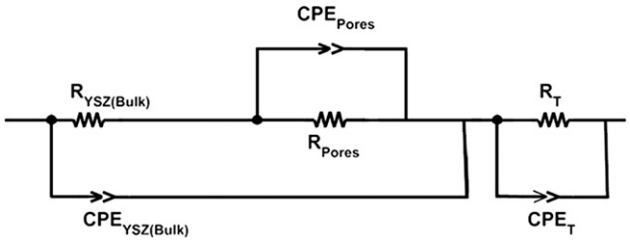

Fig. 4 An equivalent circuit of the sprayed YSZ.

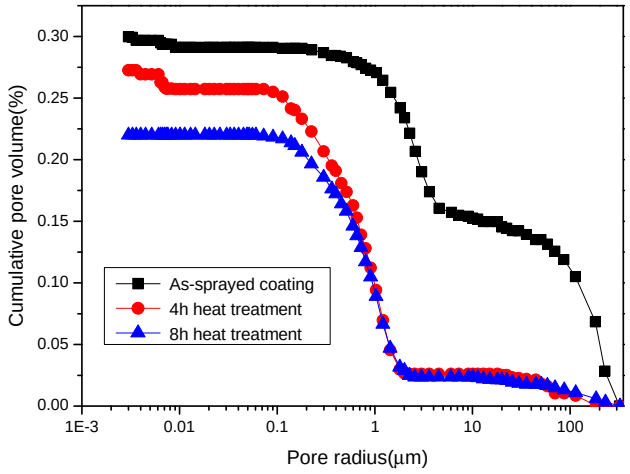

Fig. 5 Porosity of the YSZ coatings measured at different times at 1250 °C.

YSZ (RP · CP) whose frequency range is approximately 1 Hz, and the charge transfer resistance that is masked by the frequency of $1–10^{-2}$ MHz [25]. The equivalent circuit presented here is different from the previous equivalent circuits reported in some literature [18–22]. As described in the literatures, the two semicircles in Nyquist plots from the origin are the resistances of grain and grains boundaries. But in author's opinion, for the APS coating, the microstructure is quite non-uniform and especially displays bimodal structures for the YSZ coating and the grains and grain boundaries are not clear. Porous structure is an important characteristic of APS coating. According to the typical microstructure of APS, the bimodal distribution in YSZ seems suitable for APS. Furthermore, the simulation results by the circles together with a measured spectrum are shown in Fig. 2b. The simulation results in Fig. 2 are in good agreement with the measured results. Based on it, the spectra are fitted with an equivalent circuit model, which represents the microstructural features of the materials under examination [18]. It means that the equivalent circuit in this experiment is very well suitable for the APS YSZ coating.

3.2. The relation between the sintering behaviors and the electrical properties

When exposed to the high temperature air, the YSZ coating begins to sinter. The change of porosity is one of the important signs of sintering [24]. In Fig. 5, the porosity of

as-sprayed YSZ coating is ~29.97% then after 4 h heat treatment, the porosity decreased to ~27.26% and ~22.03% after 8 h. This results suggests that the micro-pores (≤ 1 μm) in the coating healed quickly when sintering happened.

Nyquist plots for different heat treatment times are presented in Fig. 6. Each plot consists of two semi-circles with different diameters, the first semi-circle from coordinate origin is mainly corresponding to the resistance of YSZ and the second semi-circle is corresponding to the resistance of pores in the coating. With the exception of the electrode effect characterized by the tail part in the low frequency range, the overall resistance, which is represented by the intercept on the real impedance axis [14], changes sharply from as-sprayed state to 8 h. In the Nyquist plot, the frequency decreases from the right-hand side to the left-hand side. The two semicircles are the responses from YSZ ceramic and the pores in YSZ.

The phase angles as a function of frequency are represented in Fig. 7. For three specimens, the highest and second highest frequency relaxation has a similar relaxation frequency. As reported earlier [26], the lowest frequency relaxation stems from the electrode effect rather than the material being investigated and the highest and second highest frequency relaxations are the responses from the ceramic bulk and the pores of the YSZ coating, respectively.

The resistance of the YSZ ceramic bulk as a function of heat treatment times is represented in Fig. 6. Evidently, the resistances of YSZ ceramic decreased with the increasing heat treatment times. For the pores in YSZ coating, the resistance exhibits the same tendency in the specimens subjected to 8 h heat treatment. Contrary to the case of resistance, the capacitance values of the ceramic and the pores increased with the heat treatment times, indicating the sintering behavior of the coating.

The resistance obtained from the simulation circle was therefore taken as the measured result [27]. This electrochemical impedance was simulated with AC equivalent circuit to determine the resistance and capacitance (CPE) of material constituents. The impedance of a CPE, Z_{CPE}, is given by

$$Z_{CPE} = \frac{1}{A(j\omega)^n} \tag{1}$$

where A is a parameter independent of frequency. When the exponential factor $n=1$, the CPE functions as an ideal

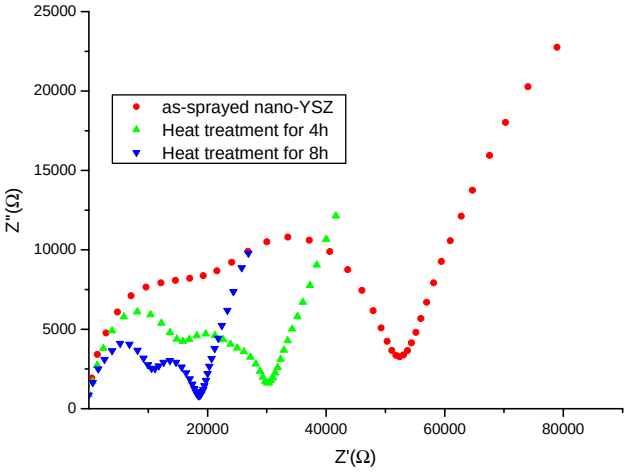

Fig. 6 Nyquist plots of impedance spectra of the YSZ coatings exposed to 1250 °C air for different times.

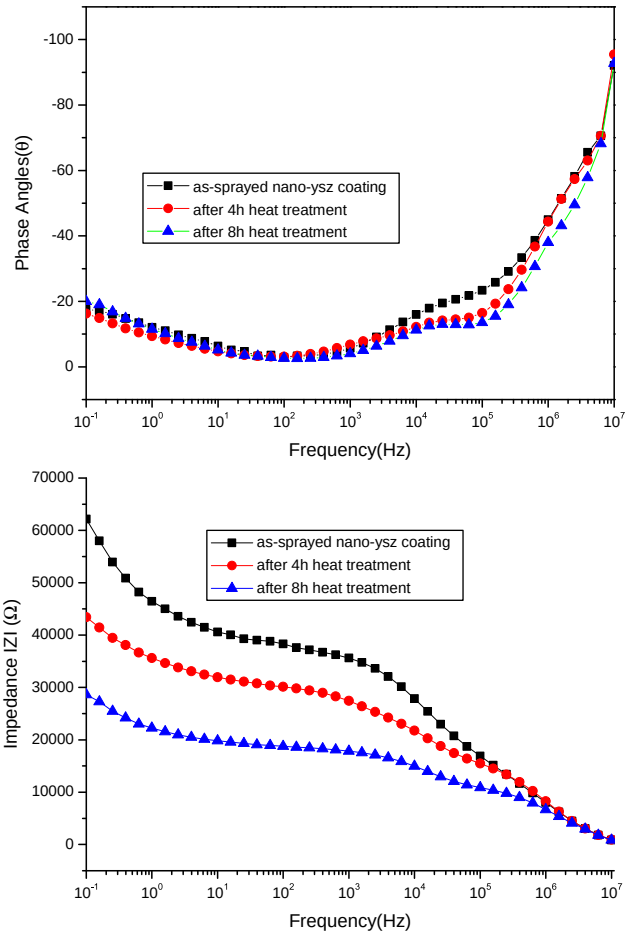

Fig. 7 Bode plots of the YSZ coatings exposed to 1250 °C air for different times.

capacitor and A are therefore equal to the capacitance C. In most cases, n is less than 1. It should be noted that n is a mathematical factor without physical meaning (i.e. it acts as a fitting parameter), but it represents an effective approach to complicated relations among several elements (R, C, etc.). In general, the resistance and capacitance are associated with chemical inhomogeneity and geometrical non-uniformity, which causes frequency dispersion [28]. In the case of non-ideal capacitive response, the value of A cannot be used to represent the capacitance of the system. Here we adopt an equivalent capacitance C, which may be acquired by [29,20]

$$C = R^{(1-n)/n} A^{1/n} \tag{2}$$

The capacitance can be achieved using Eq. (2). The variation tendencies of resistance and capacitance with different heating times in early stage are shown in Fig. 8. From Fig. 8, it can be seen that the resistance of YSZ monolith and pores in YSZ decreased with the heat treatment times and the capacitance increased. When the free standing YSZ coating was exposed to 1250 °C in air, the shrinkage occurred [24]. Usually the resistance is dependent on the length cross sectional area of materials. The resistance plot fits the regular pattern. The capacitance can be derived by

$$C = \frac{\varepsilon S}{4\pi k d} \tag{3}$$

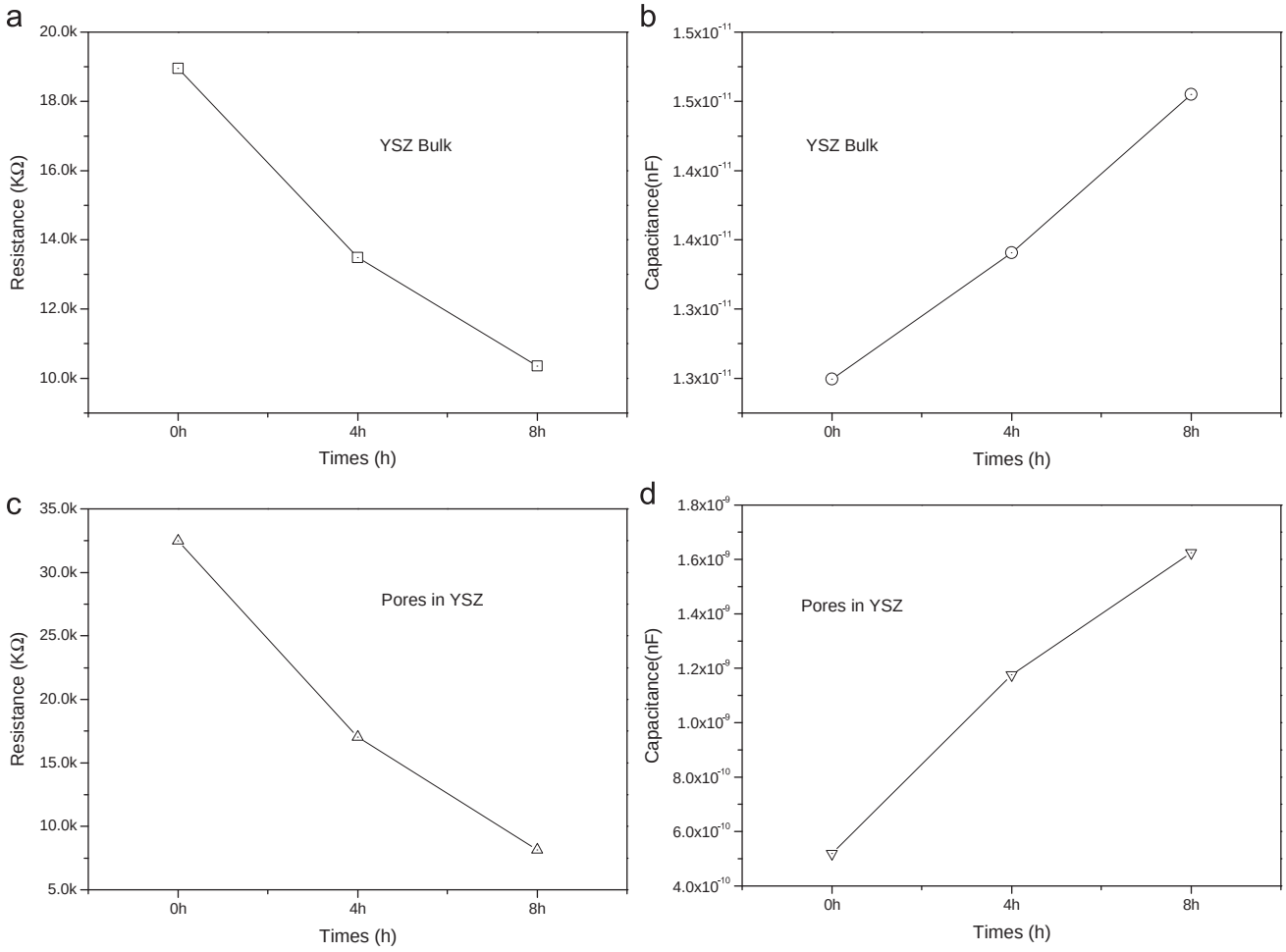

Fig. 8 Electrical properties of YSZ coating: resistance (a) and capacitance (b) of YSZ bulk; resistance (c) and capacitance (d) of pores in YSZ coatings as a function of heat treatment in 1250 °C.

where ε is a material constant, S is the opposite area of capacitor, k is the static power constant and d is the electrode distance. Obviously, d decreases and S increases when the sintering occurs. Finally, the sintering behavior of free standing YSZ coating can be characterized by AC impedance. And the variation tendency for AC impedance is that the resistance decreases and capacitance increases with the times at the early stage. Especially, the transition rates for the molten parts and semi-molten parts are quite different, which is originated from the sintering counteraction of semi-molten parts in YSZ coating. And therefore, the different sintering behavior can be estimated quantitatively.

3.3. Changes in electrical properties with the CMAS deposits infiltration

It has been found that in the present study CMAS melt and infiltrate into the YSZ coating rapidly during the samples exposed at 1250 °C as reported by Wu et al. [6]. The samples of coating with CMAS deposits were heat treated for 4 h, 8 h, 24 h and 48 h at 1250 °C and then tested using impedance spectroscopy separately. The Nyquist and Bode plots are shown in Figs. 9 and 10, respectively, which depict the AC impedance behavior of YSZ sample with CMAS infiltration in different heat treatment periods.

The results from Fig. 9 show that after different heat treatment periods with CMAS infiltration, the Nyquist plots still consist of two semi-circles (the molten parts and semi-molten parts in YSZ coating). It can be seen that when the CMAS infiltrated into the YSZ coating for 4 h, the plot is similar to that of YSZ for 4 h heat treatment without CMAS infiltration. However, when the samples were exposed at 1250 °C for 8 h, 24 h and 48 h, there was a significant variation in the plots. The experimental results showed that the first semicircle became smaller and the second semicircle became more and more larger in proportion. From the Bode plots in Fig. 10b, the plot values at the range of 10^{-1}–10^{2} Hz represent the YSZ coatings resistance and it can be identified from the AC impedance behavior of the samples [17]. All plots for different heat treatment periods showed an increasing tendency in resistances of YSZ coating with the heat treatment periods when CMAS infiltrated.

On the basis of the Nyquist plots, there are still two semicircles in the spectra of all CMAS infiltration samples, and hence it can be simulated based on a model of two R–C components [20]. The equivalent circuit model to fit the measured impedance spectra was established same as

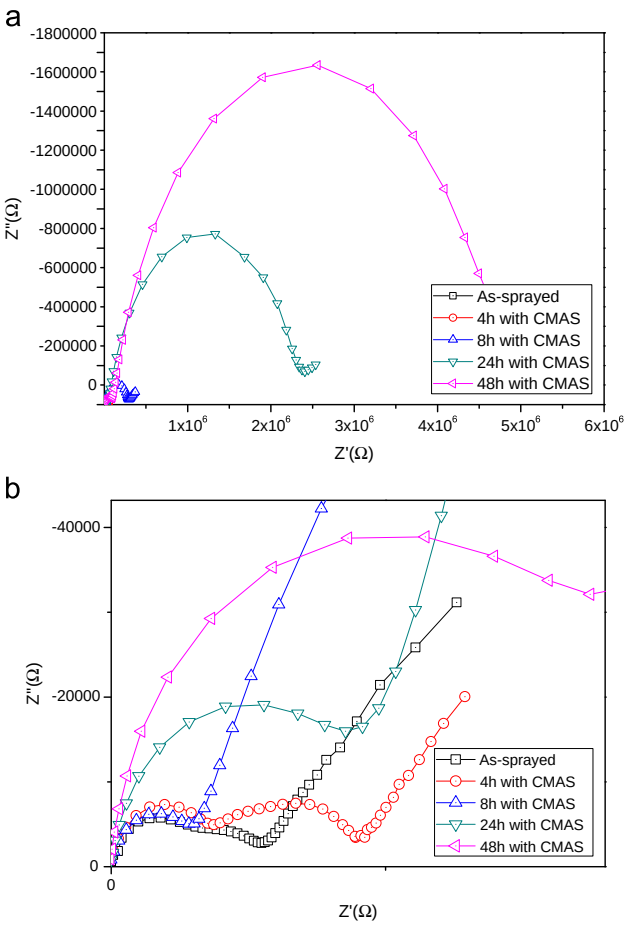

Fig. 9 Nyquist plots of impedance spectra measured after TBC exposed to 1250 °C air with CMAS deposits for different times.

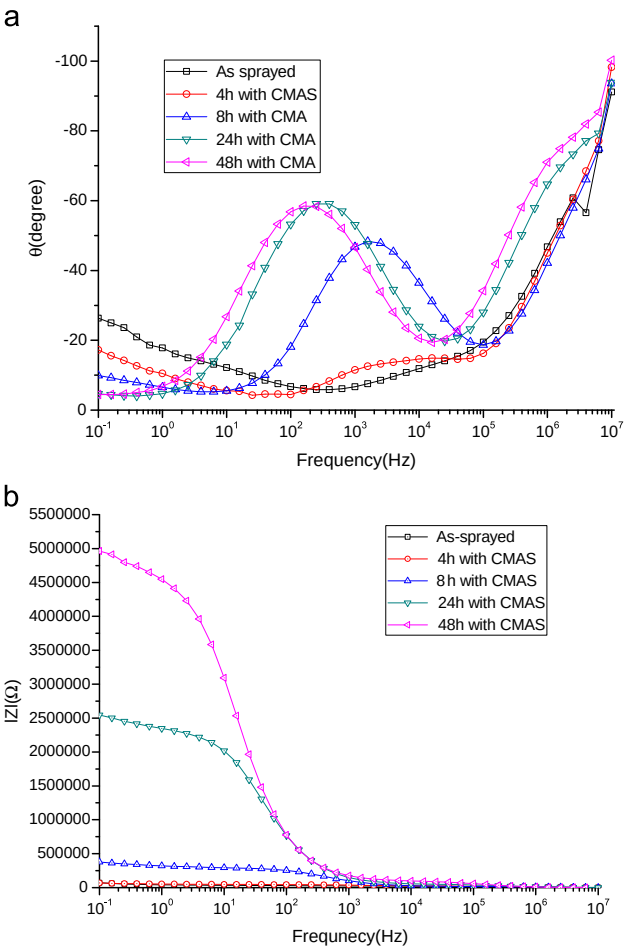

Fig. 10 Bode plots of impedance spectra measured after TBC exposed to 1250 °C air for different times.

presented in Fig. 3. With this model, a typical fitted result is shown in Fig. 11, which is in good agreement with the measured result affirming the authenticity of the proposed model.

The resistance and capacitance of the CMAS infiltration YSZ coatings with different exposure times 1250 °C at 1250 °C are represented in Fig. 12. Obviously, the resistance of YSZ bulk in the free standing coating with CMAS infiltration increased. There is a slight decrease of resistance from 0 h to 4 h and then slight increase up to 8 h followed by a sharp increase in resistance for 24 h and 48 h exposure at the temperature of 1250 °C. The experimental results showed that the capacitance of YSZ bulk exhibited the same tendency before 24 h, then decreased sharply in the case of exposure at 1250 °C for 48 h. However, the capacitance of pores, contrary to YSZ bulk, increased from 0 h to 4 h significantly, then it decreased up to 8 h, then increased followed again by a drop in resistance with the exposure period from 24 h to 48 h. This phenomenon may be closely associated with the CMAS infiltration into the YSZ coating, which causes the internal microstructure change, and this can also be explained by Eqs. (2) and (3).

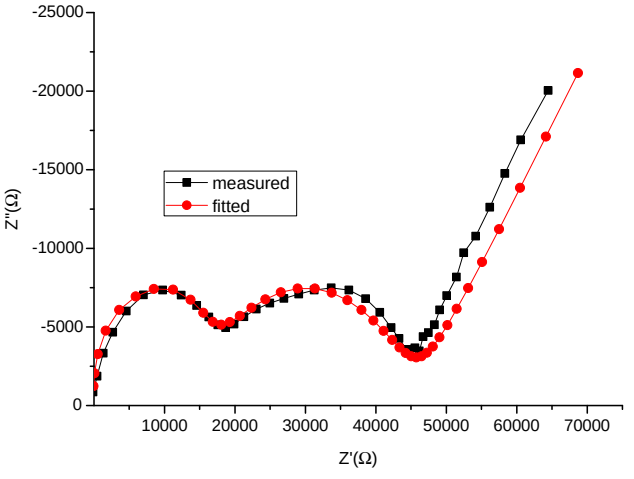

Fig. 11 Measured Nyquist impedance spectra (a) and fitted result (b) of with CMAS deposits after 4 h heat treatment at 1250 °C.

4. Conclusions

Electrochemical impedance spectroscopy can be used to study the microstructure evolution behavior of air plasma sprayed YSZ coating with CMAS deposits. The result of the AC equivalent circuit revealed that the molten part and the semi-molten part in YSZ coating have the different resistance and capacitance change rates, i.e., the resistance and capacitance

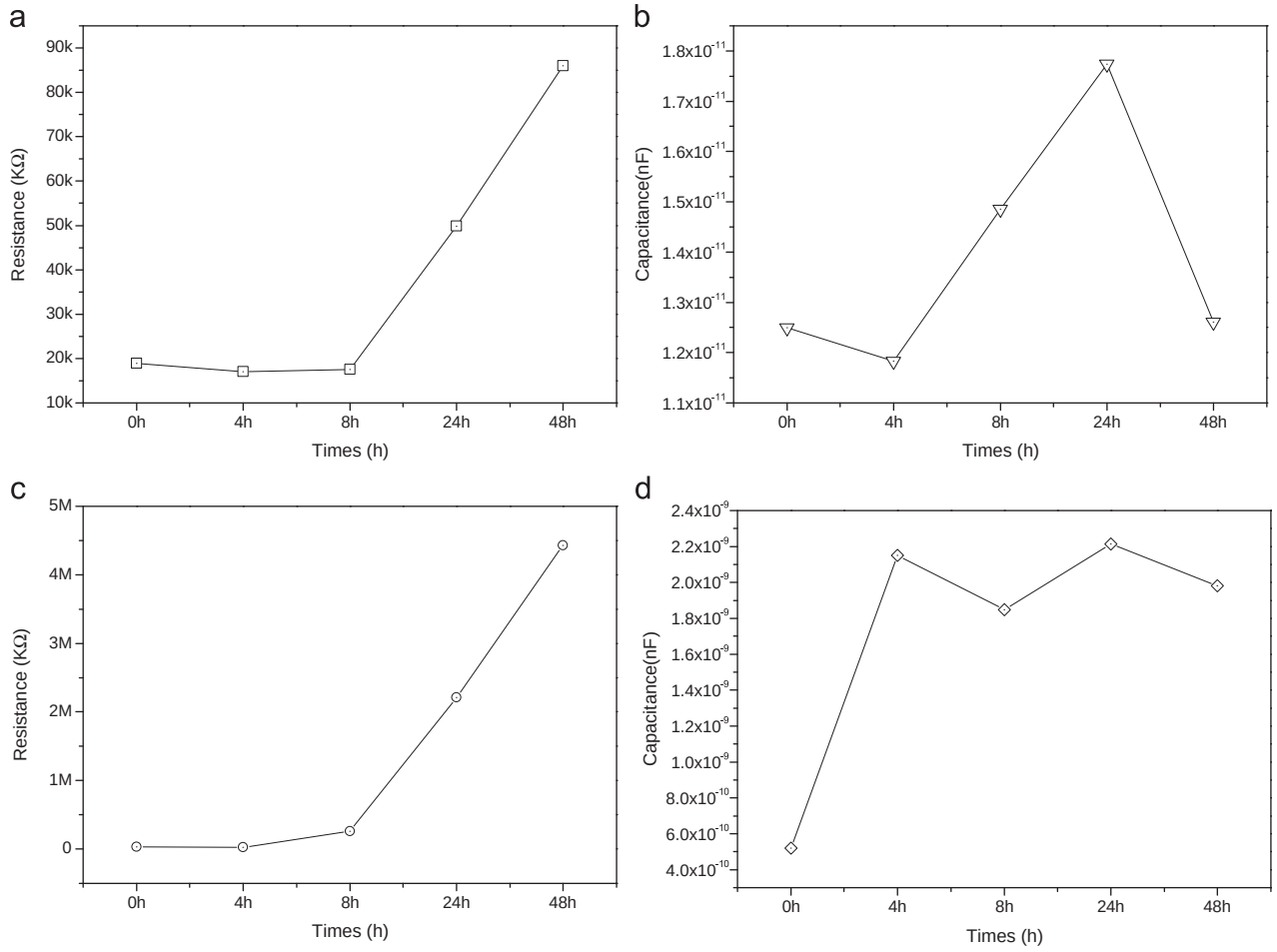

Fig. 12 Electrical properties of YSZ coating: resistance (a) and capacitance (b) of YSZ bulk; resistance (c) and capacitance (d) of pores in YSZ coatings as a function of heat treatment in 1250 °C with CMAS deposits.

change rate of the semi-molten part is higher than that of the molten part, suggesting the different sintering behavior of the two parts in coating with CMAS deposits. The different sintering rate will cause the stress instability failure of the coating. Therefore, EIS is a new way for investigating CMAS deposits' influence on the coatings.

Acknowledgments

This research is sponsored by the New Century Excellent Talents in University (NCET) and National Nature Science Foundation of China (NSFC, nos. 50771009 50731001).

References

[1] N.P. Padture, M. Gell, E.H. Jordan, Thermal barrier coatings for gas-turbine engine applications, Science 296 (2002) 280.
[2] M.J. Stiger, N.M. Yanar, M.G. Toppings, et al., Thermal barrier coatings for the 21st century, Metallkd 90 (1999) 1069.
[3] R.A. Miller, Thermal barrier coatings for aircraft engines: history and directions, Journal of Thermal Spray Technology 1 (1997) 35.
[4] C.G. Levi, Emerging materials and processes for thermal barrier systems, Solid State and Materials Science 1 (2004) 77.
[5] J. Wu, H.B. Guo, Y.Z. Gao, et al., Microstructure and thermophysical properties of yttria stabilized zirconia coatings with CMAS deposits, Journal of the European Ceramic Society 31 (10) (2011) 1881.
[6] M.P. Borom, C.A. Johnson, L.A. Peluso, Role of environmental deposits and operating surface temperature in spallation of air plasma sprayed thermal barrier coatings, Surface and Coatings Technology 86–87 (1996) 116.
[7] F.H. Stott, D.J. Wet, R. Taylor, Degradation of thermal-barrier coatings at very high temperatures, MRS Bulletin 10 (1994) 46.
[8] J. Kim, M.G. Dunn, A.J. Baran, et al., Deposition of volcanic materials in the hot sections of two gas turbine engines, Journal of Engineering for Gas Turbines and Power 7 (1993) 641.
[9] J.L. Smialek, F.A. Archer, R.G. Garlick, Turbine airfoil degradation in the Persian Gulf war, JOM Journal of the Minerals Metals and Materials Society 46 (1994) 39.
[10] C. Mercer, S. Faulhaber, A.G. Evansand, et al., A delamination mechanism for thermal barrier coatings subject to calcium–magnesium–alumino-silicate (CMAS), Acta Materialia 53 (2005) 1029.
[11] S. Krämer, J. Yang, C.G. Levi, et al., Thermochemical interaction of thermal barrier coatings with molten CaO-MgO-Al_2O_3-SiO_2 (CMAS) deposits, Journal of the American Ceramic Society 89 (2006) 3167.
[12] L. Li, D.R. Clarke, Effect of CMAS Infiltration on Radiative Transport Through an EB-PVD Thermal Barrier Coating, International Journal of Applied Ceramic Technology 5 (2008) 278.
[13] X. Chen, Calcium-magnesium-alumina-silicate (CMAS) delamination mechanisms in EB-PVD thermal barrier coatings, Surface and Coatings Technology 200 (2006) 3418.

[14] A. Aygun, A.L. Vasiliev, N.P. Padture, Novel thermal barrier coatings that are resistant to high-temperature attack by glassy deposits, Acta Materialia 55 (2007) 6734.
[15] P. Mohan, T. Patterson, B. Yao, et al., Environmental degradation of thermal barrier coating and mitigation by electrophoretically deposited overlay, Journal of Thermal Spray Technology 1–2 (2010) 156.
[16] L. Li, Hitchman, N.J. Knapp, Failure of thermal barrier coatings subjected to CMAS attack, Journal of Thermal Spray Technology 1–2 (2009) 148.
[17] J. Zhang, V. Desai, Evaluation of thickness, porosity and pore shape of plasma sprayed TBC by electrochemical impedance spectroscopy, Surface and Coatings Technology 190 (2005) 98.
[18] M.D. Shawkat, S.H. Song, P. Xiao, Evaluation of degradation of thermal barrier coatings using impedance spectroscopy, Journal of The European Ceramic Society 22 (2002) 101.
[19] X. Wang, J. Mei, P. Xiao, Non-destructive evaluation of thermal barrier coatings using impedance spectroscopy, Journal of the European Ceramic Society 21 (2001) 855.
[20] S.H. Song, P. Xiao, An impedance spectroscopy study of high-temperature oxidation of thermal barrier coatings, Materials Science and Engineering B 97 (2003) 46.
[21] L.F. Deng, Y.S. Xiong, P. Xiao, Modelling and experimental study of impedance spectra of electron beam physical vapour deposition thermal barrier coatings, Surface and Coatings Technology 201 (2007) 7775.
[22] L.F. Deng, P. Xiao, Characterisation of alumina scales on Fecralloy using impedance spectroscopy, Thin Solid Films 516 (15) (2008) 5027.
[23] R.S. Lima, A. Kucuk, C.C. Berndt, Bimodal distribution of mechanical properties on plasma sprayed nanostructured partially stabilized zirconia, Materials Science and Engineering A 327 (2002) 224–232.
[24] J. Wu, H.B. Guo, L. Zhou, L. Wang, et al., Microstructure and thermal properties of plasma sprayed nanostructure YSZ thermal barrier coatings, Journal of Thermal Spray Technology 6 (2010) 1186.
[25] B. Jayaraj, V.H. Desai, C.K. Lee, et al., Electrochemical impedance spectroscopy of porous ZrO_2-8 wt.% Y2O3 and thermally grown oxide on nickel aluminide, Materials Science and Engineering A 372 (2004) 278–286.
[26] J. Zhang, V. Desai, Evaluation of thickness, porosity and pore shape of plasma sprayed TBC by electrochemical impedance spectroscopy, Surface and Coatings Technology 190 (2005) 98.
[27] S.H. Songa, P. Xiao, L.Q. Weng, Evaluation of microstructural evolution in thermal barrier coatings during thermal cycling using impedance spectroscopy, Journal of The European Ceramic Society 25 (2005) 1167.
[28] S.T. Amaral, I.L. Muller, Effect of silicate on passive films anodically formed on iron in alkaline solution as studied by electrochemical impedance spectroscopy, Corrosion 55 (1999) 17.
[29] T. Jacobsen, B.C. Zachau, L. Bay, et al., SOFC cathode mechanisms, in: F.W. Paulsen, N. Bonanos, S. Linderoth, M. Mogensen, B. Zachau-Christiansen (Eds.), High-temperature Electrochemistry: Ceramics and Metals, Proceedings of the Seventeenth Riso International Symposium on Materials Science, RI, 1996, p. 29.